Drug Design, Development and Therapy Dovepress

Open Access Full Text Article ORIGINAL RESEARCH

Network Pharmacology and Metabolomics Reveal Anti-Ferroptotic Effects of Curcumin in Acute Kidney Injury

Xi Liu[1,2,*], Yu Zhou[3,*], Ziyi Lu[1], Fenglin Yang[1], Yizhi Wang[4], Sijin Zhang[5], Jinwen Zhang[1], Hong Zou[6], Min Lin[1]

[1]Research Center of Innovation, Entrepreneurship, Minjiang University, Fuzhou, 350100, People's Republic of China; [2]Key Laboratory for Chemical Biology of Fujian Province, MOE Key Laboratory of Spectrochemical Analysis and Instrumentation, College of Chemistry and Chemical Engineering, Xiamen University, Xiamen, 361005, People's Republic of China; [3]Cancer Research Center & Jiangxi Engineering Research Center for Translational Cancer Technology, Jiangxi University of Chinese Medicine, Nanchang, Jiangxi, 330004, People's Republic of China; [4]School of Intelligent Science and Control Engineering, Jinling Institute of Technology, Nanjing, 211169, People's Republic of China; [5]Guangdong Cardiovascular Institute, Guangdong Provincial People's Hospital, Guangdong Academy of Medical Sciences, Guangzhou, 510000, People's Republic of China; [6]Physical Education Department, Xiamen University, Xiamen, 361005, People's Republic of China

*These authors contributed equally to this work

Correspondence: Min Lin; Hong Zou, Email minlin@mju.edu.cn; zou_hong0402@126.com

Introduction: Acute kidney injury (AKI) is linked to high rates of mortality and morbidity worldwide thereby posing a major public health problem. Evidences suggest that ferroptosis is the primary cause of AKI, while inhibition of monoamine oxidase A(MAOA) and 5-hydroxytryptamine were recognized as the defender of ferroptosis. Curcumin (Cur) is a natural polyphenol and the main bioactive compound of *Curcuma longa*, which has been found nephroprotection in AKI. However, the potential mechanism of Cur in alleviating AKI ferroptosis remains unknown.

Objective: This study aims to investigate the effects of Cur on AKI ferroptosis.

Methods: Folic acid (FA)-induced AKI mouse model and erastin/(rsl-3)-induced HK-2 model were constructed to assess the renoprotection of Cur. The nuclear magnetic resonance (NMR)-based metabolomics coupled network pharmacology approach was used to explore the metabolic regulation and potential targets of Cur. Molecular docking and enzyme activity assay was carried out to evaluate the effects of Cur on MAOA.

Results: Our results showed that in vivo Cur preserved renal functions in AKI mice by lowering levels of serum creatinine, blood urea nitrogen, while in vitro ameliorated the cell viability of HK-2 cells damaged by ferroptosis. Mechanistic studies indicated that Cur protected AKI against ferroptosis via inhibition of MAOA thereby regulating 5-hydroxy-L-tryptophan metabolism.

Conclusion: Our study for the first time clarified that Cur might acts as a MAOA inhibitor and alleviates ferroptosis in AKI mice, laying a scientific foundation for new insights of clinical therapy on AKI.

Keywords: acute kidney injury, curcumin, network pharmacology, metabolomics, monoamine oxidase A, ferroptosis

Introduction

AKI is a serious condition in clinical inpatients linked to high morbidity and mortality rates.[1] It is marked by a rapid deterioration in glomerular function and buildup of metabolic waste products, for example urea nitrogen and creatinine.[2,3] The importance of AKI in the development of the disease is often overlooked. Along with other complications, such as heart failure, kidney injury, and sepsis, one or more episodes of AKI favor the development of chronic kidney disease, thereby increasing the mortality rates.[3,4] Studies have shown that the pathophysiology of AKI is linked to immunological imbalance, inflammatory response, oxidative stress, and apoptosis.[5–7] Pathologically, AKI severely damages renal tubular cells, causing apoptosis and necrosis with renal dysfunction.[8] Although AKI is reversible, there is currently no effective clinical treatment. Currently, the available therapeutic strategies for AKI are mainly

Received: 3 September 2024
Accepted: 13 December 2024
Published: 21 December 2024

symptomatic, and effective interventions based on pathological mechanisms remain to be discovered. Recent years, ferroptosis, a form of cell death characterized by iron-dependent accumulation of lipid peroxide, has been demonstrated to play a key role in the development of AKI.[9] The tryptophan metabolite 5-HT has been found to exert anti-iron death effects in a very different manner from cystine, whereas monoamine oxidase A (MAOA) enhances cellular iron death sensitivity by degrading 5-HT.[10] Many small molecules targeted to inhibit ferroptosis, such as baicalein[11] and silymarin,[12] have been found to have clear AKI ameliorating effects, thus suggesting that targeting iron death may provide new insights into clinical therapeutic strategies for AKI.

Herbs or monomers characterized by high potency, low toxicity and multi-targeting have received much attention for the prevention and treatment of ferroptosis-related diseases, especially AKI.[13,14] Curcumin (Cur) is a natural polyphenol and the main bioactive compound of *Curcuma longa*, exerts immunoregulatory, anti-inflammatory, antioxidant, and anti-apoptotic effects.[15–18] Extensive research demonstrated the remarkable therapeutic effects of Cur on various kidney diseases.[19–21] And it has been reported that Cur reverses the decline in renal function in patients with AKI by modulating the immune response, reducing inflammatory response and apoptosis, and inhibiting oxidative stress.[22–24] Several clinical trials have demonstrated the therapeutic potential of Cur in cardiovascular disease, diabetes, and cancer.[25,26]

In addition, Cur has been found to play a role in ameliorating ferroptosis-related diseases by inhibiting LOX, modulating mitochondrial oxidative stress, and ferritin autophagy.[14,27] However, the role of Cur's anti-ferroptosis effects in AKI treatment is still unknown. Considering the multiple beneficial effects of Cur in AKI treatment, it is important to identify its molecular targets. This information is essential for the future expansion of the practical application of Cur in AKI treatment.

Metabolomics is a sub-discipline of systems biology that uses high-throughput methods for the qualitative or quantitative analysis of metabolites. This approach is used to monitor the dynamic changes in metabolites that reflect the state of the body.[28–30] The metabolome reflects the terminal variation of the pathological or physiological state, genetically controlled intrinsic metabolism, and environmental influences (eg, diet and medicine).[28,31,32] Therefore, metabolite profiling provides information regarding the disorder-related changes in certain biochemical pathways.[33,34] Recent evidence indicated that a significantly metabolic dysregulation caused by hypoxia and mitochondrial dysfunction is closely related to AKI.[35] However, metabolomics falls short in elucidating the endogenous mechanisms that drive alterations in metabolites during AKI, such as the upstream pathways, protein interactions, and metabolite biosynthesis involved.

Network pharmacology is a systematic approach based on network analysis of a biological system to select specific nodes that assist in designing multi-target drug molecules.[36] It is designed to investigate the relationship among drugs, targets, pathways, and diseases by constructing a multi-level network model.[37] In recent years, network pharmacology has gained significant popularity as a powerful tool for identifying active ingredients in drugs, predicting specific mechanisms underlying drug actions, analysing major active ingredient targets, and developing combination drugs.[38–40] Nonetheless, network pharmacology only suggests potential targets and pathways of active compounds, lacking confirmation of the combination and effects that Cur exerts on targets. Consequently, the complementary use of metabolomics and systematic network pharmacology prediction could provide new strategies to clarify the potential mechanisms responsible for the action of Cur in the treatment of AKI.

In this research, we conducted such a combined approach to excavate the targets and potential molecular mechanisms of Cur in treating AKI. We identified related targets and metabolic responses that show inhibition of ferroptosis play an important effect in the Cur-treated FA-induced mouse model. This research provides novel insights into the renoprotective effects of Cur in the management of AKI.

Materials and Methods

Chemicals and Reagents

Curcumin (Cur), folic acid (FA), RSL-3, and Erastin were acquired from MedChemExpress (Monmouth Junction, NJ, USA). Deuterium oxide (D2O) was obtained from Qingdao Tenglong Weibo Technology Co., Ltd. (Qingdao, China). 3-(trimethylsilyl) propionate-2, 2, 3, 3-d4 (TSP) was acquired from Sigma (St Louis, MO, USA). Methanol and

chloroform were obtained from Sinopharm (Shanghai, China). Cell Counting Kit-8 kit was acquired from Beyotime (Shanghai, China). Monoamine oxidase (MAO) Activity Assay Kit was acquired from Solarbio Technology Co., Ltd. (Beijing, China). The malondialdehyde (MDA) and tissue iron assay kit were acquired from Nanjing Jiancheng Bioengineering Institute (Nanjing, China).

Animal Experiment

The SPF (Specific Pathogen Free) C57BL/6 mice (Male, 8 weeks-old) were acquired from Shanghai SLAC Animal Company (Shanghai, China). All mice were kept in a controlled environment with a room temperature of 23±3°C and relative humidity of 70±5% under SPF conditions. They were subjected to a 12-hour dark-light cycle and provided with ad libitum access to food and water to promote their well-being and reduce stress. The study protocol received approval from the Ethics Review Committee of Xiamen University (XMULAC20220200). All animal experiments were conducted in accordance with the animal care and use guidelines of Xiamen University (Xiamen, China).

After 1 week of acclimatization, all mice were completely and randomly assigned to three groups (N=10 per group): control, FA-treatment (model), and Cur-treatment groups. The AKI model was established by administering a single intraperitoneal injection of FA (200 mg/kg) as previously described.[41] The control group received the same volume of saline. Cur (dose: 100 mg/kg) was administered immediately along with the modelling and three consecutive times within 24 h (ie, with 8-h intervals). All mice were euthanized at 24 h, and both kidneys and blood samples were obtained for subsequent analysis.

Detection of Blood Urea Nitrogen (BUN) and Creatinine (CRE)

Serum BUN and CRE (N=10) were detected to monitor renal function, as previously reports.[21,41] The blood sample was collected and placed at room temperature in a centrifuge tube for 30–60 minutes. Subsequently, the blood sample was centrifuged at 14,000 g for 15 minutes, the separated serum was placed into a clean centrifuge tube, and centrifugation was repeated (14,000 g for 3 minutes) to remove any remaining cells. The obtained serum was used to detect BUN and CRE levels by a commercial reagent kit from Solarbio Technology Co., Ltd. (Beijing, China) (Urea Nitrogen/Urea Content Assay Kit, Cat: BC1535. Creatinine Content Assay Kit, Cat: BC4915). The testing was conducted in accordance with the instructions provided by the manufacturer.

Histopathological Assessment

The kidneys were fixed in 4% phosphate-buffered formaldehyde to maintain their structure, dehydrated, and then embedded in paraffin. Following serial sectioning (thickness: 5 μm), paraffin-embedded sections were subjected to staining by haematoxylin and eosin. Images were acquired using an inverted microscope (AE31E; Motic, Xiamen, China), with 5 photographs acquired for each sample.

Samples Preparation of Nuclear Magnetic Resonance (NMR)-Based Metabolomics

Kidney samples (~100 mg) (N=10 per group) were added to 1.5 mL of extract solution (water: chloroform: methanol =2.85:4:4) and subjected to homogenization at a frequency of 65 hz for a duration of 60 seconds to extract aqueous metabolites. After vortexing for 5 minutes, the sample was centrifuged at speed of 12,000 g (4°C, 15 minutes), and the methanol was removed by nitrogen bubbling. The aqueous phase was lyophilized, and redissolved in 600 μL of 50 mm phosphate buffer contained 0.1 mm TSP (pH 7.4, 100% D_2O,). The redissolved sample was centrifuged at speed of 12,000 g (4°C, 15 minutes) to obtain the supernatant, which was carefully transferred to NMR tubes and centrifuged at 4°C (1500 g, 5 minutes) prior to NMR detection.

NMR Detection and Data Processing of NMR-Based Metabolomics

The one-dimensional ^{1}H-NMR spectra were obtained from an 850 MHz NMR spectrometer (Bruker AVANCE III HD, Bruker BioSpin, Ettlingen, Germany) using a NOESYGPPR1D pulse sequence at 25°C. The experimental parameters used for NMR detection were as follows: spectral width: 20 ppm, relaxation delay: 4 s and 32 scans. MestReNova 9.0 software obtained from Mestrelab Research S.L. (Santiago de Compostela, Spain) was utilized to process NMR data,

including phase correction, baseline correction. The chemical shifts of the spectrum were referenced to TSP (δ 0.00). The data matrix was obtained using MATLAB R2014b (MathWorks, Natick, MA, USA) by binning the δ 9.5–0.75 spectral region at 0.001 ppm and normalising all the peak integrals according to the peak integrals of the TSP. This was followed by removal of the δ 4.85–4.75 region. The version 8.3 of Chenomx NMR Suite (Chenomx Inc., Edmonton, Canada), Human Metabolome Database (accessed at http://www.hmdb.ca/ on 1 January 2023), and related reported sources were combined to perform resonance assignments of metabolites. The verification of resonance assignments was validated by two-dimensional ^{1}H-^{13}C heteronuclear single quantum correlations (HSQC) spectrum (Supplementary Figure 1).

Multivariate Statistical Analysis and Pathway Analysis of NMR-Based Metabolomics

Multivariate statistical analysis of the data matrix was conducted on the SIMCA14.1 software package (MKS Umetrics, Malmö, Sweden). Firstly, unsupervised principal component analysis (PCA) was conducted to illustrate the clustering trends for the group separation. Furthermore, supervised partial least squares-discriminant analysis (PLS-DA) was utilized to maximally discriminate the metabolic fingerprinting of kidneys. Rigorous permutation tests of 200 cycles were subsequently proceed to acquire the interpretive (R^2) and predictive abilities (Q^2) for evaluating the reliability of the PLS-DA model. Significantly altered metabolites ($p<0.05$) were identified by the IBM SPSS Statistics 22.0 software (IBM, Armonk, NY, USA). The MetaboAnalyst 5.0 web server (accessed at http://www.MetaboAnalyst.ca on 1 January 2023) was used to visualise pathway enrichment, and critical metabolic pathway screening criteria were based on two criteria (ie, pathway impact value [PIV] >1 and $p<0.05$).

Network Pharmacology Construction

The version 3.8.2 of Cytoscape software (Cytoscape Consortium, San Diego, CA, USA) was utilized to obtain the metabolite-protein-pathway network and reveal the core metabolites and associated proteins. The disease-associated candidate targets were gained from the GeneCards (https://www.genecards.org/), OMIM (https://omim. org/), TCMSP (http://tcmspw.com/tcmsp.php), and therapeutic target database (TTD; http://db.idrblab.net/ttd/) through a search using the keyword 'acute kidney injury'. The potential targets of Cur were screened through a search using the keyword "Curcumin" in the SwissTargetPrediction (http://www.swisstargetprediction.ch/), BATMAN-TCM (http://bionet.ncpsb.org/batman-tcm/), STITCH 5.0 (http://stitch.embl.de/) and ChEMBL (https://www.ebi.ac.uk/chembl/). The predicted target of Cur against AKI was considered to be in the overlap of the drug targets and disease targets. The KEGG (Kyoto Encyclopedia of Genes and Genomes) pathway and GO (Gene Ontology) enrichment analyses of potential targets were conducted by Cytoscape using the ClueGO plugin unit. Import the differential metabolites identified from metabolomics and predicted target of Cur against AKI into Cytoscape, and use Metscape to form an interaction network for visualize the interactions among the genes, enzymes, pathways, and metabolites.

Molecular Docking

The molecular docking analysis was conducted utilizing the Schrödinger software. The molecular structure of Cur (PubChem CID 969516) was gained from PubChem Compound (https://www.ncbi.nlm.nih.gov/pccompound), and was transformed from the native format into pdbqt format using Maestro–LigPrep. The crystal structures of target proteins, including monoamine oxidase A (MAOA; Protein Data Bank identifier [PDB ID]: 2Z5Y), glutaminase 1 (GLS1; PDB ID: 3VOY), and glutaminase 2 (GLS2; PDB ID: 4BQM), were gained from PDB database (the Research Collaboratory for Structural Bioinformatics, https://www.rcsb.org/). The obtained protein crystals were optimized by protein preprocessing, regenerate states of native light, H-bond assignment optimization, protein energy minimization, and deletion of water. We used the SiteMap module in Schrödinger to predict the best binding sites, and then used the Receptor Grid Generation module in Schrödinger to set the most suitable Enclosing box to wrap the predicted binding site, and on the basis of which we obtained the active side. Subsequently, molecular docking was performed at the active site and molecular mechanics with generalised Born and surface area solvation (MM-GBSA) computational analysis to assess the stability of ligand-protein binding. Extra precision (XP) Gscore and MM-GBSA dG Bind were used to determine the stability of ligand-protein binding. Finally, PyMOL was utilized to visualize the ligand protein binding with the optimal scores.

Enzyme Activities Assay

The kidney samples were processed according to the instructions provided in the commercial assay kits (Monoamine Oxidase Activity Assay Kit, Beijing Solarbio Technology Co., Ltd., CAT: BC0015). Extraction solution (sample weight [g]: extraction solution [mL] = 1:1.5) was added to prepare the samples (N=6 per group) for testing. Next, the reagents were added in sequence according to the instructions and read using a microplate reader (BioTek, Winooski, VT, USA) at 360 nm wavelength at 10s and 2h. Ultimately, the results on enzyme activity were normalized depending on the tissue weight.

qPCR

TriZol (Takara, Kyoto, Japan) was utilized to extract total RNA on the basis of the procedures provided by the manufacturer. Total RNA (1 μg) (N=3 per group) was utilized to cDNA synthesis using the ReverTra Ace qPCR RT Master Mix (LabLead, Beijing, China). The cDNA was utilized to amplify specific target genes using the SYBR Green Real-time PCR Master Mix (TOYOBO). RT-PCR was conducted as follows: 95°C for 10 min, followed by 95°C for 10s, 60°C for 30s, and 95°C for 10s for 39 cycles. The data were measured and exported using CFX96TM Real-Time System (BIO-RAD). The delta cycle threshold (Ct) ($2^{-\Delta\Delta Ct}$) approach was utilized to estimate the relative gene expression levels. The data were normalized to those obtained for the internal control β-actin. The primers used for qPCR were acquired from Sangon Biotech Co., Ltd. (Shanghai, China), including MAOA: 5'-GACCTTGACTGCCAAGATT-3' and 5'-GATCACAAGGCTTTATTCTA-3' and β-actin: 5'-CTTCCAGCCTTCCTTCCTGG-3' and 5'-CTGTGTTGGCGTACAGGTCT-3'.

Cell Culture

Human kidney tubular epithelial cells (HK2) were gained from ATCC (Manassas, VA, USA). The cells were cultured in DMEM (high glucose; HyClone) containing 10% foetal bovine serum (Biological Industries), streptomycin (100 μg/mL), and penicillin (100 IU/mL) (Thermo Fisher Scientific, Waltham, MA, USA) biochemical incubator at 37°C and supplemented with 5% CO_2.

Cell Counting Kit-8 Experiment

HK2 cells were seeded in 96-well plates at a density of 5×10^3/well and cultured for 12 hours with 200 μL of medium. After reaching an appropriate 80–90% confluency, the culture media were supplemented with 2 μM RSL-3 or 2 μM Erastin to induce ferroptosis. Moreover, HK2 cells (N=5 per group) were supplemented with different final concentrations of Cur (50, 25, 10, 5, 1, and 0.1 μM) for 24 h. Subsequently, each well was added with 10% (volume/volume) of Cell Counting Kit-8 reagent. After incubated at 37°C for 2–4 h, Multi-mode microplate readers (POLARstar Omega, BMG LABTECH GmbH, Germany) was used to detect the absorbance at 450 nm wavelength.

Lipid Peroxidation Assessed

Tissue samples (N=5 per group) were assayed on the basis of the instructions of MDA Assay Kit (Beijing Solarbio Technology Co., Ltd). Microplate readers was used to measure the MDA levels at 530 nm wavelength, which reflect the degree of lipid peroxidation in ferroptosis.

Analysis of Tissue Iron Content

Tissue samples (N=5 per group) were analyzed for iron content utilizing iron assay kit (Nanjing Jiancheng Bioengineering Institute) based on the provided protocol. Iron levels were determined at 520 nm wavelength using multi-mode microplate readers.

Statistical Analysis

The Data were expressed as the mean ± standard deviation (SD) and p-values <0.05 indicate statistically significant differences. Differences among groups were assessed by one-way ANOVA utilizing IBM SPSS Statistics 22.0 software (IBM), followed by the post hoc analysis of Tukey's multiple comparison test for homoscedasticity and Games-Howell

for heteroscedasticity. Statistical significance is indicated as follows: *p<0.05, **p<0.01, ***p<0.001, ****p<0.0001. GraphPad Prism 8.0.2 software (GraphPad Software Inc., San Diego, CA, USA) was used to draw graphs.

Results

Cur Treatment Alleviated Renal Injury in Mice with FA-Induced AKI

FA-induced AKI has been described in humans,[42] and the animal model recapitulates most of the human AKI pathologies observed in the clinic,[43] including oxidative stress, inflammation, and renal cell death and regeneration. To assess the renoprotective effect of Cur, we established an AKI model induced by a high dose of FA and injected Cur for treatment. The schematic diagram shown in Figure 1A illustrates the experimental procedure of FA-induced AKI and drug administration. Cur significantly reduced the levels of CRE and BUN, which are indicators of renal function. These levels were elevated in the FA-induced AKI model (Figure 1B and C). Haematoxylin-and-eosin staining of kidney sections indicated that Cur significantly reduced histological damage to the kidneys (Figure 1D). Taken together, these data suggested that Cur could protect against functional acute renal malfunction and structural organ injury.

Cur Remodelled the Metabolite Profiles in the Kidneys of AKI Mice

The non-targeted metabolomics analysis identified a total of 41 metabolites from ^{1}H NMR spectrum recorded on control, FA-treatment, and Cur-treatment groups of kidneys aqueous extracts (Table S1). Typical one-dimensional ^{1}H spectrum was shown in Figure 2. Two dimensional ^{1}H-^{13}C-HSQC spectrum was recorded to confirm the resonance assignments of the metabolites (Figure S1).

Firstly, we established the unsupervised PCA model to visualize and comprehensively assess the metabolic patterns of the three groups of kidneys. The PCA model showed that all points were situated in the circle, representing the 95% confidence interval (Figures 3A–C). We founded that samples from the same group showed a clustering trend, whereas those from the three different groups of kidneys exhibited obvious separation (Figure 3A). The metabolic profile was well

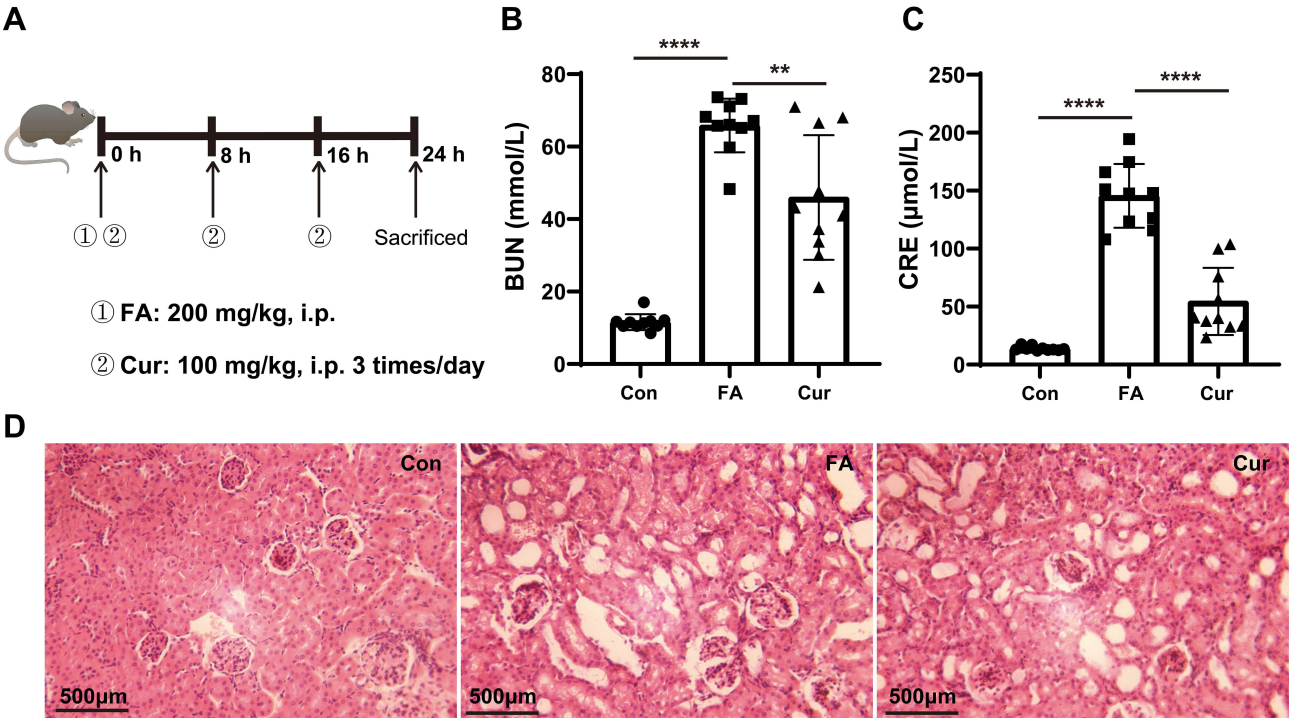

Figure 1 Curcumin exerted renoprotective effects in folate-induced AKI. (**A**) Schematic representation of the folic acid-induced (FA-induced) AKI model and drug treatment. (**B** and **C**) Blood urea nitrogen (BUN) and creatinine (CRE) levels in mice with FA-AKI. (**D**) Representative haematoxylin-eosin staining of kidneys. The scale bar represents 500 μm. Experimental data are presented as mean ± SD. Statistical significances (N=10): $p < 0.01$, **; $p < 0.0001$, ****. Each repeat was performed as a separate, independent experiment or observation.

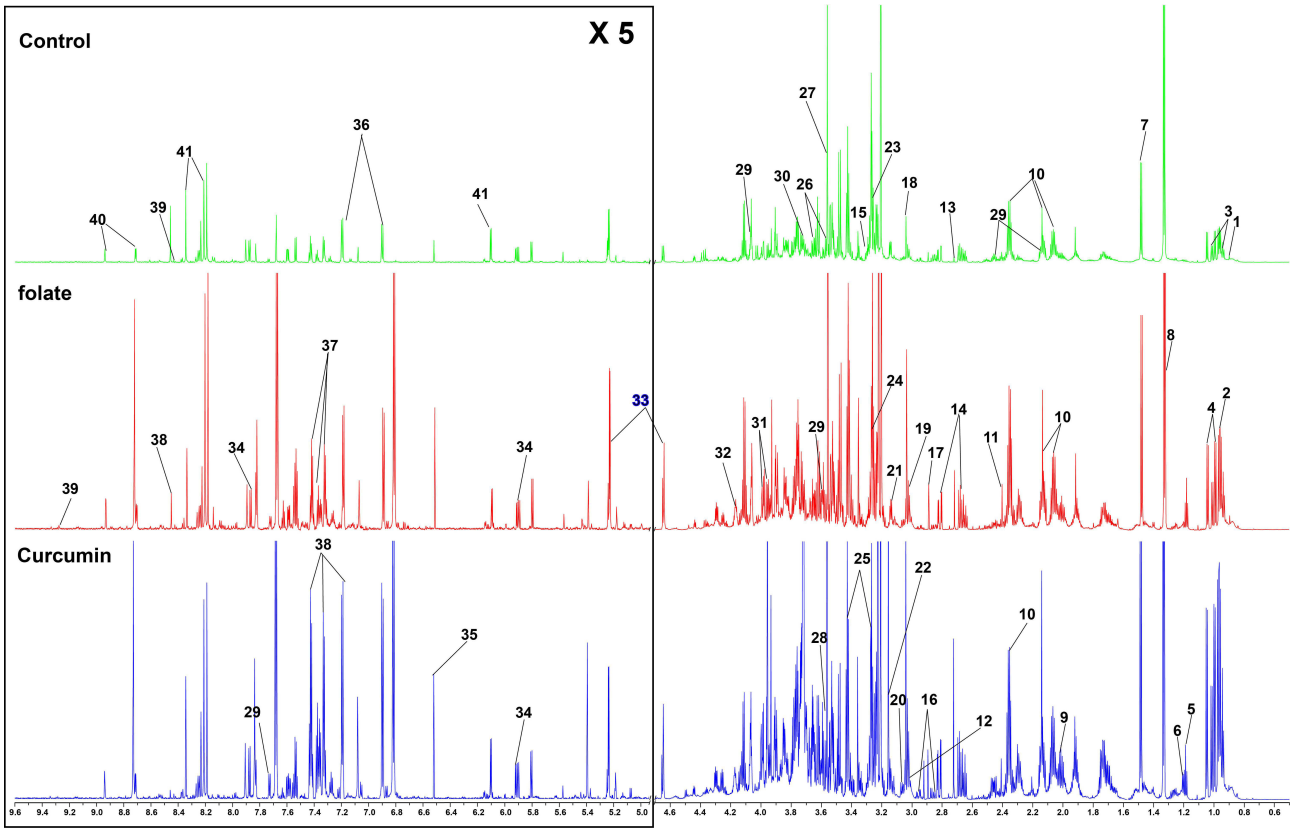

Figure 2 Typical one-dimensional (1D) ^{1}H spectrum of kidney aqueous extracts. The region of H_2O (4.75–4.85 ppm) was excluded, and the region of 4.85–9.6 ppm was magnified five times compared to the region of 0.5–4.75 ppm. Numbers in the panels represent: 1. Pantothenate; 2. Leucine; 3. Isoleucine; 4. Valine; 5. Ethanol; 6. 3-Hydroxybutyrate; 7. Alanine; 8. Lactate; 9. Proline; 10. Glutamate; 11. Succinate; 12. 5-Hydroxytryptophan 13. Dimethylamine; 14. Aspartate; 15. Arginine; 16. Glutathione; 17. Trimethylamine; 18. Creatine; 19. Lysine; 20. Ornithine; 21. Ethanolamine; 22. Choline; 23. Trimethylamine N-oxide; 24. Betaine; 25. Taurine; 26. Myo-Inositol; 27. Glycine; 28. Threonine; 29. Tryptophan; 30. Glutamine; 31. Serine; 32. sn-Glycero-3-phosphocholine; 33. Glucose; 34. Uridine; 35. Fumarate; 36. Tyrosine; 37. Phenylalanine; 38. Formate; 39. NAD^{+}; 40. Niacinamide; 41. Inosine.

distinguished between FA-treatment and control mice (Figure 3A) and between Cur- and FA-treatment mice (Figure 3B), respectively (Figure 3C). These results indicate that an extremely severe metabolic dysfunction in mice with AKI induced by FA and Cur-treatment had a metabolic regulatory effect in FA-induced AKI.

In addition, the PLS-DA models were produced to magnificent the separations of the metabolic patterns and identify important metabolites. As expected, there was obvious separation between the FA-treatment with control groups (Figure 3D), as well as between the Cur- and FA-treatment groups (Figure 3E). The parameters of R2X, R2Y, and Q2 in PLS-DA between the FA-treatment and control groups were 0.935, 0.988, and 0.902, respectively. These parameters between the Cur- and FA-treatment groups were 0.914, 0.933, and 0.873, respectively. In addition, 200 permutation tests were executed to evaluate the robustness of the built model (Figure 3F and G). The higher R^2 stands for the better explanatory capacity of the established PLS-DA model, while the higher Q^2 represents the better predictive performance. The results suggested that the PLS-DA model had good explanatory and predictive performance. Thus, the model is a valid approach for the identification of important metabolites contributing to these metabolic distinctions. Based on the PLS-DA model, 11 and 10 important metabolites were screened from the FA-treatment versus control groups (Figure 3H) and Cur- versus FA-treatment groups (Figure 3I), respectively.

Screening Differential Metabolites and Important Metabolic Pathways

The relative contents of the assigned 41 metabolites were calculated according to their NMR peak integrals relative to TSP. Thereafter, a total of 27 and 20 significantly altered metabolites were selected from the pairwise comparisons of FA-treatment versus control groups and Cur- versus FA-treatment groups, respectively. This selection was conducted using

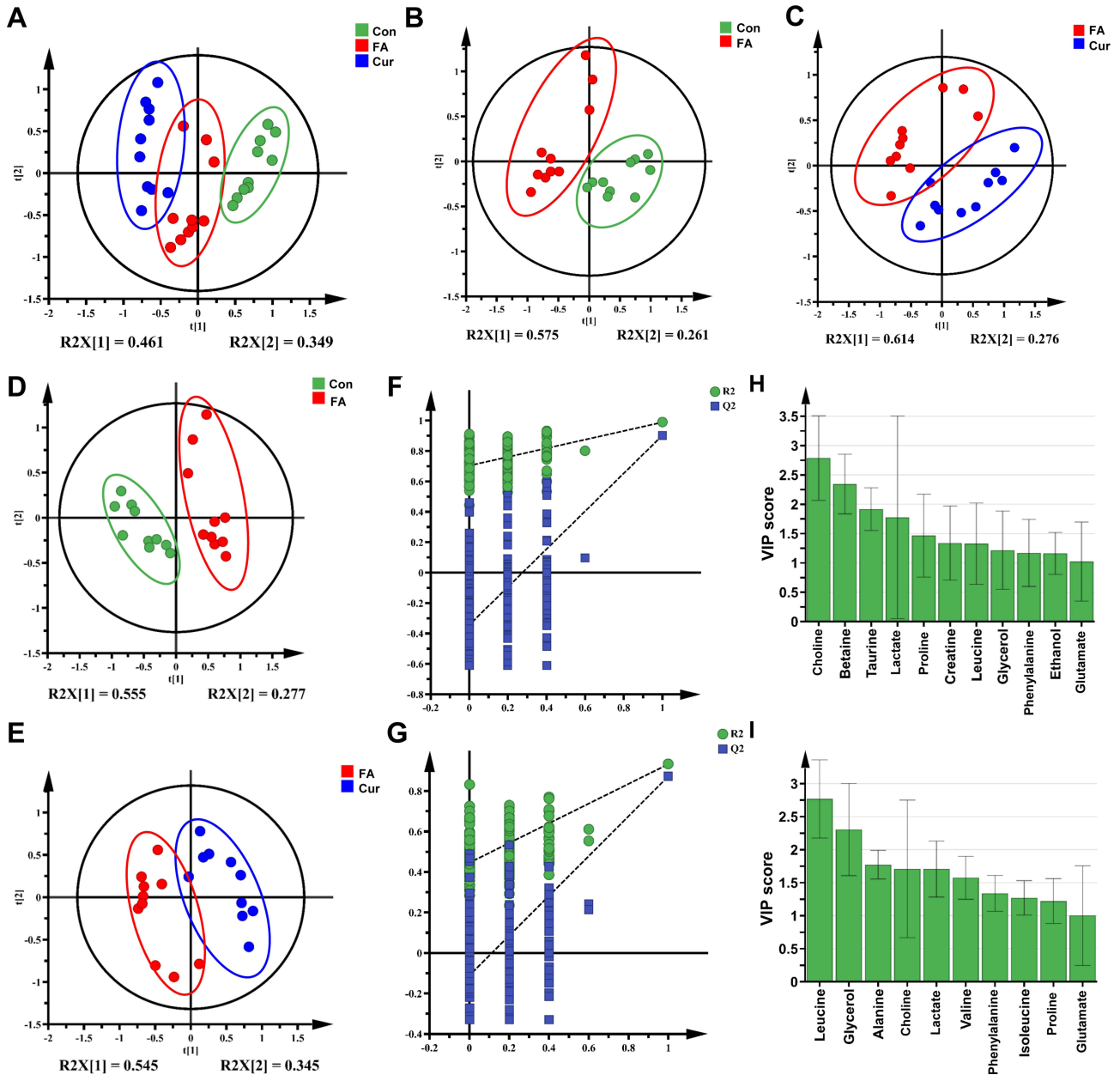

Figure 3 Multivariate statistical analysis of kidney metabolites in the control (Con), folic-acid (FA), and curcumin (Cur) groups of mice (N=10). (**A–C**) Score plot of PCA models. (**D** and **E**) Score plots of the PLS-DA models (**F**) and the permutation validation plot (**G**) for the FA versus Con groups. (**F** and **G**) Score plots of the PLS-DA models (**F**) and the permutation validation plot (**G**) for the FA versus Con groups. (**H** and **I**) The important metabolites (VIP >1) identified from the PLS-DA model of the FA vs Con (**H**) and Cur versus FA (**I**) groups.

one-way ANOVA, followed by Tukey's multiple comparison test with a criterion of p-value <0.05 (Table S2). To visualize the different levels of metabolite signatures among the control, FA-treatment, and Cur-treatment groups, the heatmap (Figure 4) was plotted based on the relative metabolic levels. Furthermore, metabolites satisfying VIP >1 or p-value <0.05 were considered characteristic metabolites associated with the therapeutic effects of Cur on AKI. In total, 30 and 24 characteristic metabolites were screened from the pairwise comparisons of FA-treatment versus control and Cur- versus FA-treatment groups, respectively. Following the intersection of the characteristic metabolites mentioned above, a total of 19 differential metabolites were screened (Table 1).

We conducted pathway analyses utilizing MetaboAnalyst 5.0 to identify the metabolic pathways according to the relative contents of the metabolites. By setting two criteria (ie, PIV >0.1 and p-value <0.05), nine and 11 metabolic

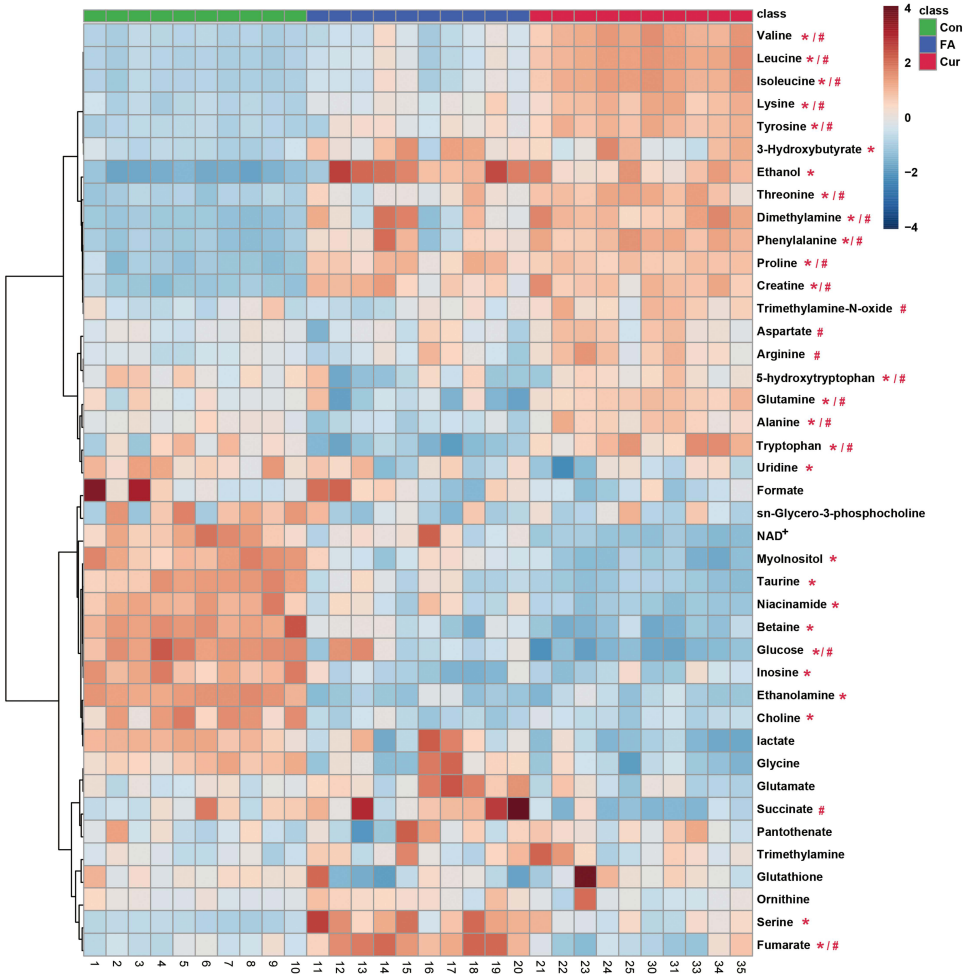

Figure 4 The heatmap analysis of the identified metabolites in the control (Con), folic acid (FA), and curcumin (Cur) groups (n=10). Significantly altered metabolites found in the FA versus Con groups are marked with "*", while those found in the Cur versus FA groups are marked with "#". Each repeat was performed as a separate, independent experiment or observation.

pathways were identified from pairwise comparisons of the FA-treatment versus control and Cur- versus FA-treatment groups, respectively (Figure 5A and B; Table S3). Metabolic pathways shared by the two comparisons were considered the most relevant to AKI and protective mechanisms of Cur. These included: Phenylalanine, tyrosine and tryptophan

Table 1 The Differential Metabolites in Kidneys of AKI Mice

Metabolites	Mean ± SD			FA vs Con	Cur vs FA	ANOVA	
	Con	FA	Cur			F	P
Leucine	1.221±0.081	1.535±0.275	2.875±0.406	↑***	↑*	89.116	<0.001
Isoleucine	0.277±0.021	0.350±0.069	0.642±0.095	↑*	↑***	74.552	<0.001
Valine	0.469±0.036	0.557±0.101	1.003±0.148	↑*	↑***	70.429	<0.001
Alanine	1.533±0.129	1.347±0.206	1.954±0.317	↓*	↑***	18.482	<0.001
Lactate	5.522±0.418	4.536±1.279	4.147±1.048	ns	ns	4.606	0.019
Proline	0.513±0.057	0.872±0.220	1.178±0.157	↑**	↑***	38.668	<0.001
Glutamate	2.060±0.170	2.297±0.428	2.265±0.389	ns	ns	1.245	0.304
5-Hydroxytryptamine	0.290±0.030	0.261±0.009	0.334±0.052	↓*	↑*	5.714	0.009
Dimethylamine	0.044±0.007	0.179±0.102	0.346±0.056	↑**	↑*	44.093	<0.001

(*Continued*)

Table 1 (Continued).

Metabolites	Mean ± SD			FA vs Con	Cur vs FA	ANOVA	
	Con	FA	Cur			F	P
Creatine	0.307±0.049	0.549±0.142	0.788±0.124	↑***	↑***	40.957	<0.001
Lysine	0.210±0.018	0.257±0.049	0.402±0.064	↑*	↑***	41.496	<0.001
Choline	4.776±1.053	3.398±0.942	3.859±0.615	↓**	ns	6.106	0.006
Threonine	0.087±0.009	0.112±0.024	0.159±0.023	↑*	↑**	30.223	<0.001
Tryptophan	1.181±0.336	0.861±0.161	1.629±0.184	↓*	↑***	28.421	<0.001
Glutamine	0.343±0.035	0.300±0.006	0.485±0.063	↓*	↑***	21.715	<0.001
Glucose	0.083±0.014	0.051±0.019	0.036±0.008	↓**	↓*	25.557	<0.001
Fumarate	0.033±0.010	0.057±0.017	0.043±0.007	↑**	↓*	9.631	0.001
Tyrosine	0.147±0.012	0.181±0.035	0.277±0.040	↑*	↑***	42.941	<0.001
Phenylalanine	0.165±0.010	0.404±0.153	0.727±0.108	↑**	↑***	60.228	<0.001

Notes: *Statistical significances (N=10):ns: no statistical significance, $p > 0.05$; *:$p < 0.05$; **:$p < 0.01$; ***:$p < 0.001$. Each repeat was performed as a separate, independent experiment or observation.

biosynthesis; Nicotinate and nicotinamide metabolism; Phenylalanine metabolism; Taurine and hypotaurine metabolism; Alanine, aspartate and glutamate metabolism; Arginine and proline metabolism; Tryptophan metabolism; Tyrosine metabolism; and Inositol phosphate metabolism.

Network Pharmacology

We executed network pharmacology analysis to further explore the mechanisms involved in the effects of Cur against AKI. Preliminary analyses were performed using the BATMAN-TCM database. The results revealed that six pathways

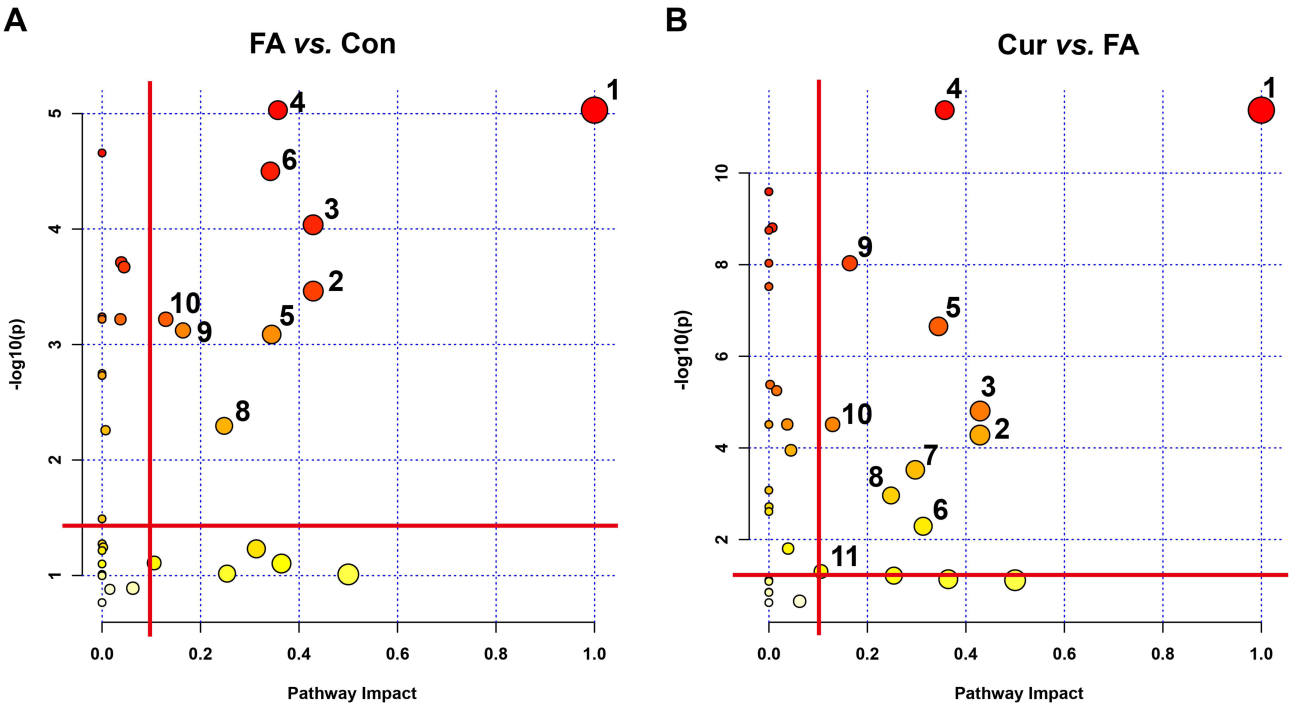

Figure 5 Metabolic pathway enrichment analysis. (**A** and **B**) Disorder metabolic pathways in the FA-induced model (**A**) regulated by treatment with Cur. Important metabolic pathways was screened by combing p-values (<0.05) and pathway impact values (PIV>0.1). Numbers in the panels stand for metabolic pathways: 1. Phenylalanine, tyrosine and tryptophan biosynthesis; 2. Nicotinate and nicotinamide metabolism; 3. Taurine and hypotaurine metabolism; 4. Phenylalanine metabolism; 5. Arginine and proline metabolism; 6. Alanine, aspartate and glutamate metabolism; 7. Glycine, serine and threonine metabolism; 8. Tryptophan metabolism; 9. Tyrosine metabolism; 10. Inositol phosphate metabolism; and 11. Glyoxylate and dicarboxylate metabolism.

were enriched in the metabolomic analysis: phenylalanine metabolism; glycine, serine and threonine metabolism; tryptophan metabolism; arginine and proline metabolism; tyrosine metabolism; and glyoxylate and dicarboxylate metabolism. These results indicated the reliability of metabolic pathway analysis.

Subsequently, we obtained 162 targets of Cur from SwissTargetPrediction, STITCH, BATMAN-TCM and ChEMBL databases and gathered 1788 targets of AKI from the TCMSP, TTD, OMIM and GeneCards databases. A total of 71 prospective targets were found, and the overlap between the drug targets and disease targets for Cur to treat AKI was visualized using a Venn diagram (Figure 6A). In addition, the compound-target network was established utilizing the Cytoscape software (Figure 6B).

To explore the potential mechanism underlying the renoprotective effects of Cur, we performed GO and KEGG enrichment analysis using ClueGO based on the overlapping targets of Cur and AKI (Figure 6C and D). GO analysis showed that the top five terms were: 1. positive regulation of lymphocyte migration; 2. positive regulation of lymphocyte chemotaxis; 3. regulation of monooxygenase activity; 4. positive regulation of mononuclear cell migration; 5. regulation of glucose import. The KEGG analysis revealed that the pathways which were significantly affected included D-amino acid metabolism, central carbon metabolism, nitrogen metabolism, phenylalanine metabolism, renal cell carcinoma, cocaine addiction, and the hypoxia-inducible factor-1alpha (HIF-1α) signaling pathway.

Analysis of Metabolomics Combined with Network Pharmacology

We sought to gain a comprehensive and systematic view of the mechanism by which Cur ameliorates AKI. Therefore, we constructed drug-reaction-enzyme-gene networks by integrating the results of metabolomics and network pharmacology (Figure 7). These networks provide insight into the overall relationship between upstream targets, pathways, and terminal metabolites. Combining the potential targets determined from network pharmacology and the differential metabolites identified from metabolomics, we selected four key upstream targets, namely MAOA, GLS1, GLS2, and acetylcholinesterase (ACHE) (Table 2). The pathways were alanine, aspartate and glutamate metabolism, tryptophan metabolism and choline metabolism, and the associated core terminal metabolites, including L-alanine, L-glutamine, L-glutamate, 5-hydroxy-L-tryptophan (5-HT), L-tryptophan, and choline. Unlike choline metabolism, alanine, aspartate, and glutamate metabolism, as well as tryptophan metabolism, were identified in the metabolomics pathway analyses. Therefore, excluding ACHE, MAOA, GLS1, and GLS2 may be essential for the renal protective effect of Cur on AKI.

Molecular Docking Between Cur and Core Target

We performed molecular docking studies using Schrödinger software to further explore the potential interaction between Cur and the core targets, including MAOA, GLS1, and GLS2. The results of molecular docking analysis are shown in Table 3. An XP Gscore <−6 indicates good binding affinity and MM-GBSA dG binding energies <−30 kcal/mol indicate stable ligand-protein binding.

The molecular docking analysis of MAOA indicated that Cur made hydrogen-bonding interactions with GLU43 and ARG51 at the active site. Moreover, Cur formed a π-Cation with ARG45 and hydrophobic interaction with TYR402, PRO274, ALA448, MET445, and TYR444 (Figure 8A and D). The binding energy of Cur on MAOA was −55.92 kcal/mol and the docking score was −8.973, indicating stable ligand-protein binding and excellent binding affinity, respectively. In molecular docking analysis of GLS2, Cur made hydrogen-bonding interactions with SER219 and LEU441, and hydrophobic interactions with ALA181, ALA180, VAL417, ALA416, and TYR399 (Figure 8B and E). The binding energy of Cur on GLS2 was −56.47 kcal/mol and the docking score was −6.023, suggesting stable ligand-protein binding and good binding affinity, respectively. For the Cur-GLS1 complex, Cur formed hydrogen-bonding interactions with TYR414, ASN388, LYS289, and LYS245, as well as hydrophobic interactions with VAL246, ALA247, TRY249 and VAL484 (Figure 8C and F). The binding energy of Cur on GLS1 was −38.01 kcal/mol and the docking score was −5.197, suggesting stable ligand-protein binding and preferable binding affinity, respectively. These results demonstrated high affinity between Cur and the core targets, especially MAOA.

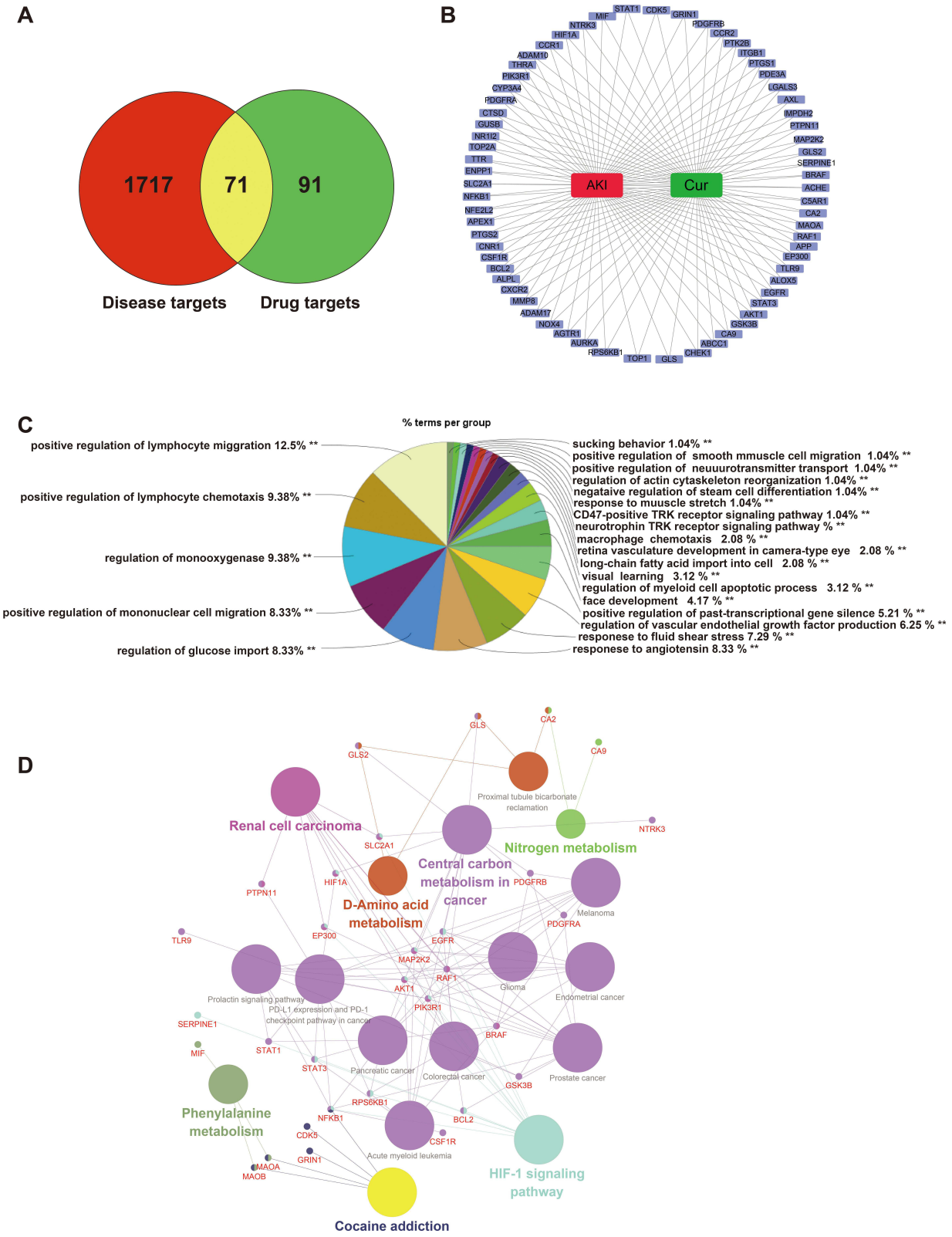

Figure 6 Network pharmacology analysis of the effects of curcumin (Cur) on acute kidney injury (AKI). (**A**) Venn diagram showing an intersection of predicted targets between Cur and AKI. Green, red, and overlapped yellow areas indicate targets for Cur, AKI, and common targets, respectively. (**B**) Compound-target network of Cur and AKI-related targets. (**C**) Gene Ontology enrichment analysis of predicted targets by using ClueGO. (**D**) Kyoto Encyclopedia of Genes and Genomes pathways enrichment analysis by using ClueGO. All pathways had a *p*-value <0.05.

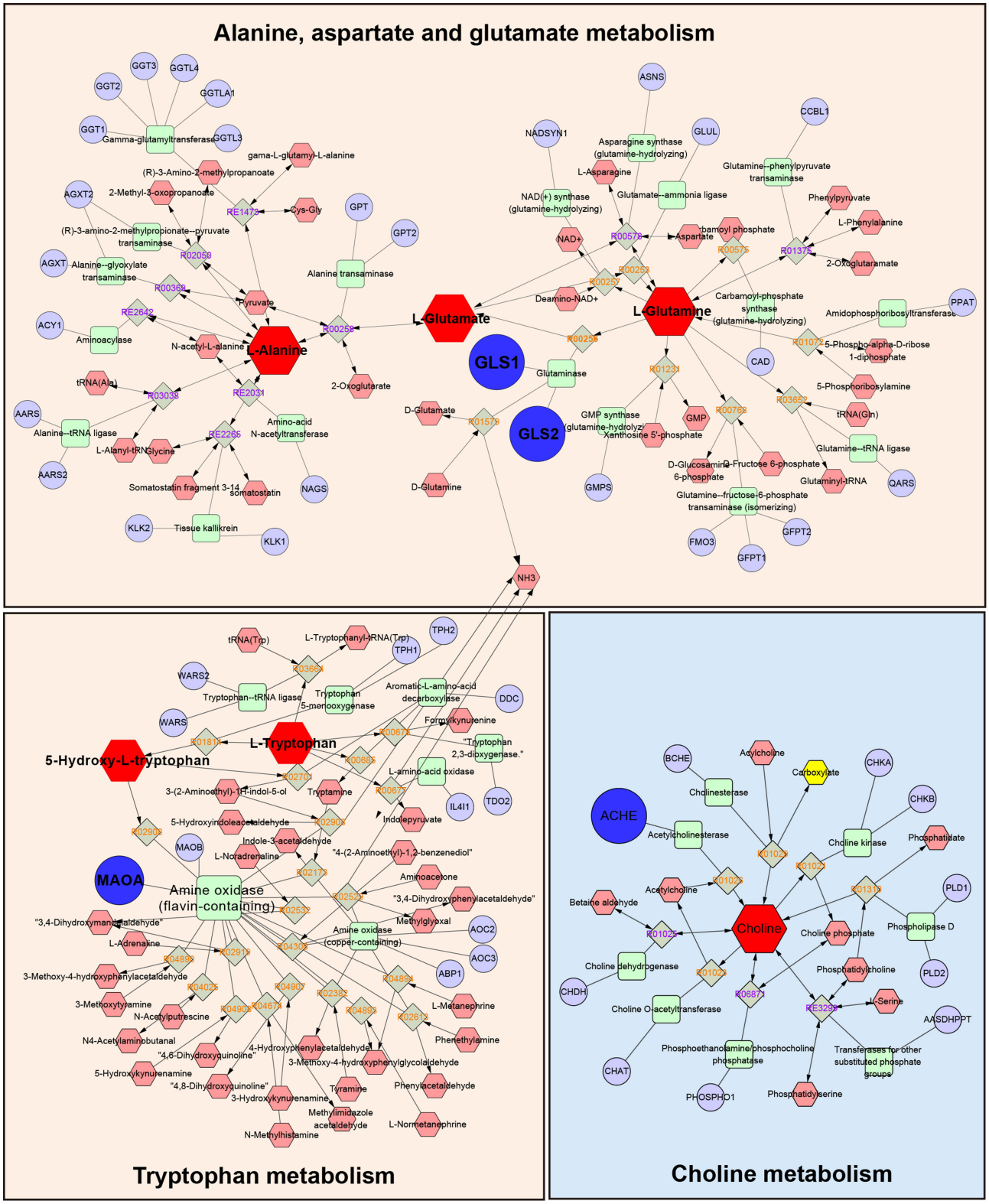

Figure 7 The interaction network among the key genes, enzymes, pathways, and metabolites. Red hexagons: active compounds; Grey diamonds: reactions; Green rectangles: proteins; Purple circles: genes. The key genes, proteins and metabolites were enlarged for emphasis. The red background highlights the significantly regulated in both the pairwise comparisons of the folic acid (FA) versus control (Con) and curcumin (Cur) versus FA groups in the metabolomics study.

https://doi.org/10.2147/DDDT.S486286 DovePress

Table 2 The Information of Core Pathways, Metabolites and Metabolites

Metabolic pathway	Target	Metabolites
Alanine, aspartate and glutamate metabolism	GLS1, GLS2	L-Alanine, L-glutamine, L-Glutamate
Tryptophan metabolism	MAOA	5-Hydroxy-L-tryptophan, L-Tryptophan
Choline metabolism	ACHE	Choline

Table 3 Molecular Docking Result of the Core Targets with Cur

CID	compound	Target	PDB ID	XP GScore	MM-GBSA dG Bind (kcal/mol)
969516	Curcumin	MAOA	2Z5Y	−8.973	−55.92
		GLS2	4BQM	−6.023	−56.47
		GLS1	3VOY	−5.197	−38.01

The Renoprotective Effect of Cur Was Closely Linked to MAOA

Previous studies have revealed that a close association between AKI and MAOA-catalyzed 5-HT degradation.[44] We sought to further investigate the possibility of MAOA as a target of CUR in the treatment of AKI. Thus, we detected the mRNA levels and enzymatic activity of MAOA in kidney tissue. As expected, the results showed that MAOA mRNA

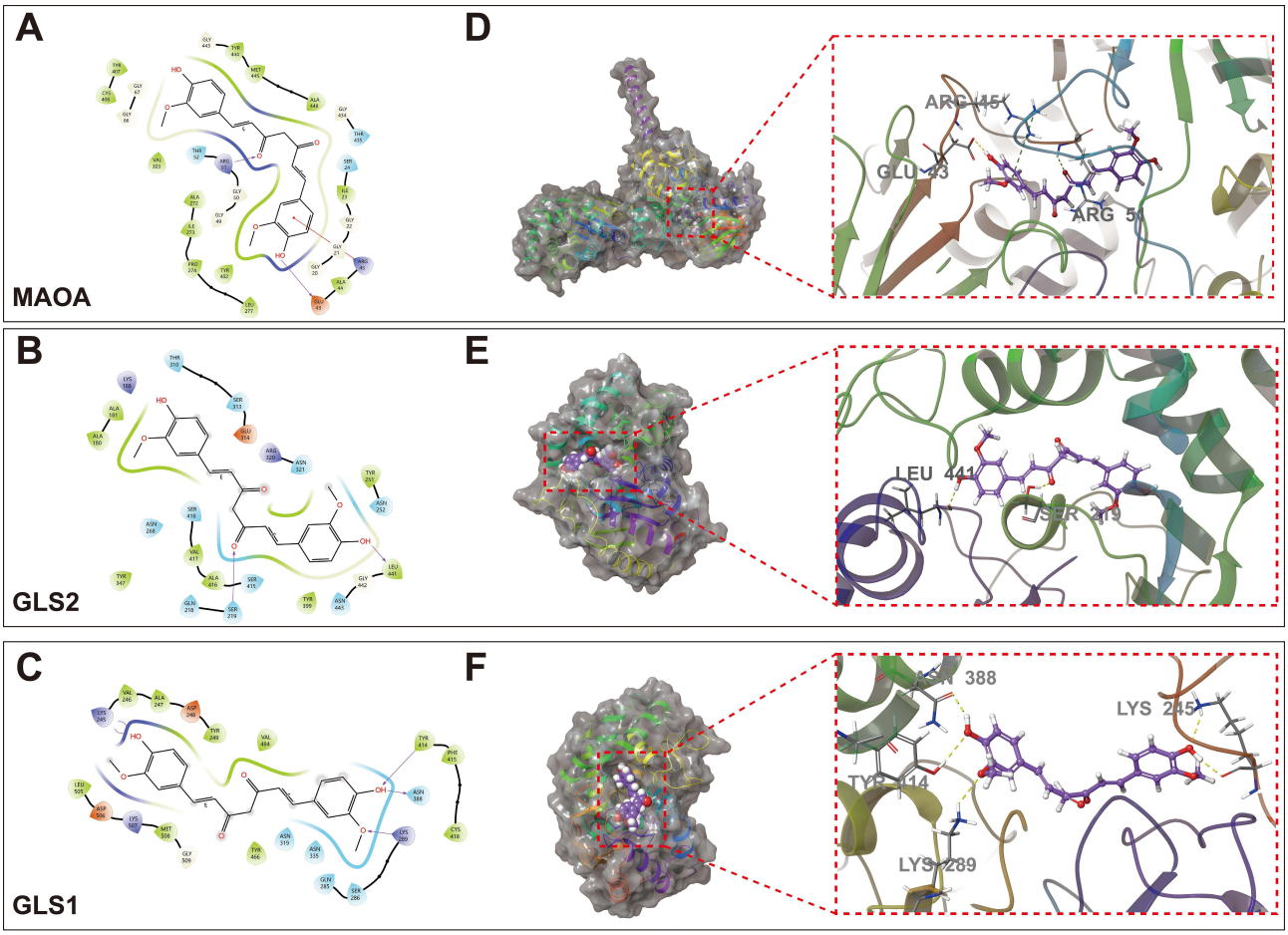

Figure 8 Molecular docking diagram of curcumin (Cur) with predicted core target proteins. (**A–C**) Two-dimensional (2D) molecular docking diagram of Cur with the key target proteins monoamine oxidase A (MAOA) (**A**), glutaminase 2 (GLS2) (**B**), and glutaminase (GLS1) (**C**). Purple arrows indicate hydrogen-bonding interactions, and red arrows indicate π-cation-bonding interactions. (**D–F**) Three-dimensional (3D) interaction diagrams of Cur and the crucial target proteins MAOA (**D**), GLS2 (**E**), and GLS1 (**F**). Yellow and green dashed lines indicate hydrogen-bonding and π-cation-bonding interactions, respectively.

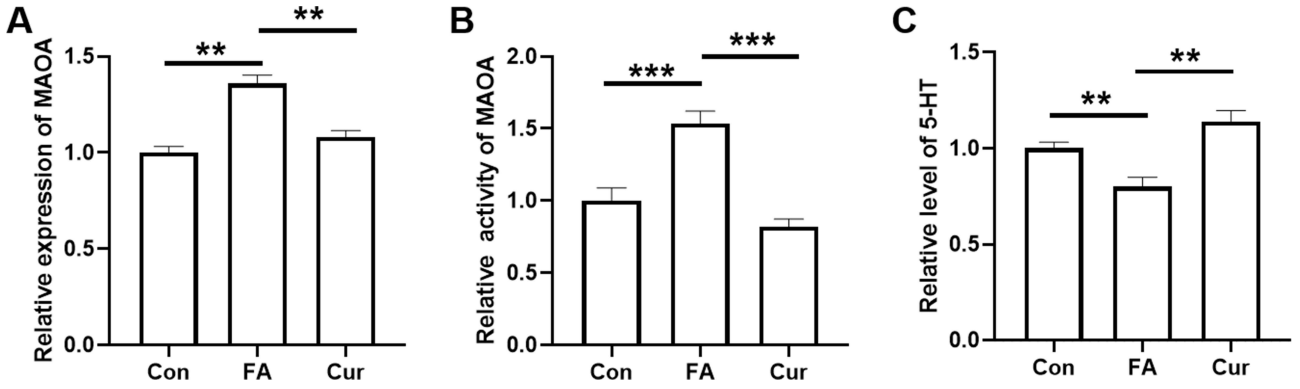

Figure 9 Effect of curcumin (Cur) on renal 5-hydroxy-L-tryptophan (5-HT) metabolism. (**A**) RT-PCR analysis of monoamine oxidase A (MAOA) mRNA levels. The mRNA levels were represented as fold change of the levels determined in the control (Con) group which normalized to those of β-actin. (**B**) Enzymatic activity of MAOA, represented as fold change of the levels measured in the Con group. (**C**) Relative levels of 5-HT, represented as fold change of the content determined in the Con group. Experimental data are presented as mean ± SD. Statistical significances (N=6): $p < 0.01$, **; $p < 0.001$, ***. Each repeat was performed as a separate, independent experiment or observation.

levels were remarkably enhanced in the FA-treatment group compared with the control group, whereas they were reduced after treatment with Cur (Figure 9A). Similarly, changes in the enzymatic activity of MAOA were observed in pairwise comparisons between the FA-treatment and control groups and between the Cur- and FA-treatment groups (Figure 9B). Furthermore, we observed a reduction in the levels of 5-HT in the FA-treatment group compared with the control group, which was reversed in the Cur-treatment group (Figure 9C). These results showed that Cur may regulate the expression and enzymatic activity of MAOA to affect 5-HT metabolism and eventually prevent AKI.

Anti-Ferroptotic Effect of Curcumin

Ferroptosis, a cell death pattern characteristic of lipid peroxidation induced by ferrous iron overload, plays a core role in the progression of AKI.[41] Extensive research has shown that inhibition of ferroptosis has a renoprotective effect in various AKI models.[45–47] Interestingly, a recent study suggested that the tryptophan metabolite 5-hydroxytryptamine (5-HT) exerts an anti-ferroptotic effect, whereas MAOA significantly abolishes the protective effect of 5-HT through its degradation.[48] Therefore, we speculated that Cur might possess anti-ferroptotic activity. To verify this hypothesis, we established a ferroptotic model of HK2 cells using RSL-3 or Erastin, and treated the cells with Cur. We found that the ferroptosis induced by RSL-3 or Erastin was reversed by treatment with 1, 5, 10, 25, and 50 μM Cur; almost complete reversal was achieved with 5 μM Cur (Figure 10A and B). We also measured the MDA levels in kidneys, which reflect the extent of lipid peroxidation (Figure 10C). The levels of iron in kidneys were also measured to assess the anti-ferroptotic effect of Cur (Figure 10D). These results suggest that Cur induces anti-ferroptosis in mice with AKI.

Discussion

AKI is a condition characterized by a decrease in renal caused by a variety of physiological and pathological factors.[4] In recent years, Cur has been extensively studied as a potential intervention for kidney disease.[16,20,22] Nevertheless, the targets and corresponding effects (eg, activation, inhibition, or invalid combination) of Cur remain unknown. In this research, the molecular mechanism of Cur against FA-AKI was investigated through the integration of metabolomics and network pharmacology. Firstly, we screened 12 differential metabolites of Cur against AKI in kidneys, and their related metabolic pathways. Secondly, by integrating metabolomics with network pharmacology, we found three core targets (MAOA, GLS1, GLS2), two related pathways (tryptophan metabolism and alanine, aspartate, and glutamate metabolism), and five key metabolites (L-alanine, L-glutamine, L-glutamate, 5-HT, and L-tryptophan). In addition, molecular docking results revealed that Cur exhibited high binding affinity to MAOA. Furthermore, our experiments verified that Cur regulated 5-HT metabolism via MAOA, thereby potentially exerting an anti-ferroptotic effect.

As a natural phenolic, Cur exhibits good pharmacological activity, including anti-cancer properties,[48] hepatobiliary protective effects[49] and renoprotective properties,[16] while with safety at high dose in humans.[50] Previous studies have

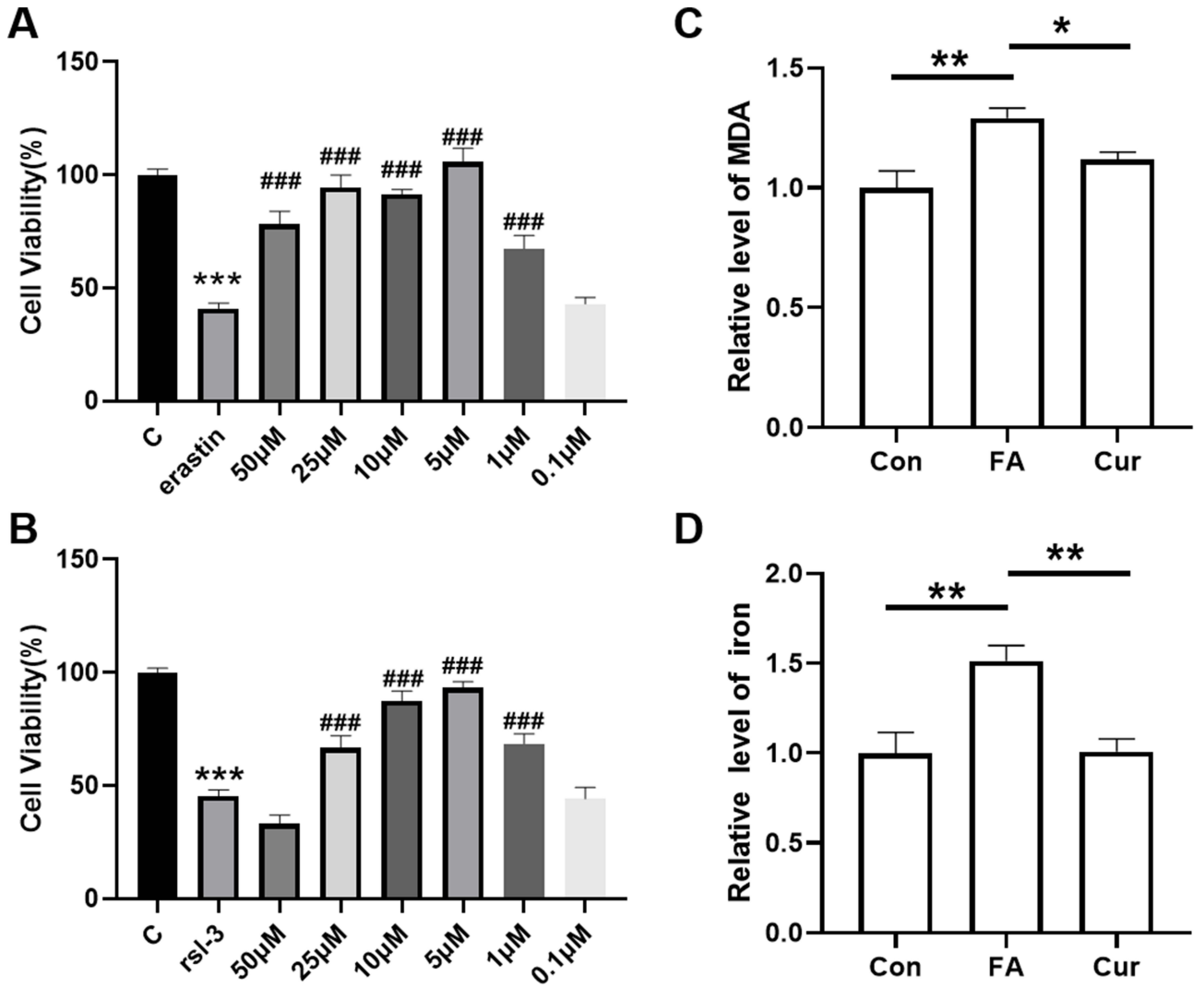

Figure 10 Curcumin (Cur) inhibited ferroptosis in HK2 cells and kidneys. (**A and B**) Cell viability assayed by CCK-8. HK2 cells were treated with 2 μM Erastin (**A**) or 2 μM RSL-3 (**B**) to induce ferroptosis, followed by treatment with Cur (50, 25, 10, 5, 1, and 0.1 μM) for 24 h. Data is presented as mean ± SD (N=5). ***: ($p < 0.001$) for statistical significances between the Control and erastin or rsl-3 groups by non-paired Student's *t*-test. ###: ($p < 0.001$) for statistical significances between the Control and Cur groups by non-paired Student's *t*-test. (**C**) Malondialdehyde (MDA) levels tested by the using MDA assay kit at 530 nm wavelength (N=5). The MDA levels, represented as fold change of the levels measured in the control (Con) group, were utilized to reflect the extent of lipid peroxidation in kidneys. (**D**) The levels of iron were measured utilizing a tissue iron assay kit (N=5). Iron levels expressed as fold change of the levels measured in the Con group. Experimental data are presented as mean ± SD. Statistical significances (N=5): $p < 0.05$, *; $p < 0.01$, **. Each repeat was performed as a separate, independent experiment or observation.

proposed possible mechanisms of Cur involved in the treatment of AKI. It was found that Cur activates the kelch-like ECH associated protein 1/Nrf2 (Keap1/Nrf2) pathway in rats with glycerol-induced AKI.[51] This activation increases the expression of antioxidant enzymes, such as NADP(H) quinone oxidoreductase 1 (NQO1), haemoglobin oxidase-1 (HO-1), and superoxide dismutase (SOD), thereby exerting antioxidant effects. In a cisplatin-induced model of AKI,[52] elevated levels of nitric oxide (NO) increased the severity of AKI. Treatment with Cur inhibited the expression and activity of nitric oxide synthase (NOS), thereby decreasing NO production. In addition, cisplatin-induced AKI was alleviated by treatment with Cur through inhibition of the nuclear factor-kappa B (NF-κB) signalling pathway and reduction of inflammatory factor release.[53]

In the present research, we explored the metabolic variations in kidneys to recognize the potential mechanisms underlying the effects of Cur in the treatment of AKI. Overall, 12 differential metabolites and 11 significant metabolic pathways were identified from metabolomics (Table 1 and Figure 5). These data displayed that the regulation of metabolism exerts a key effect in the activity of Cur against AKI. Regrettably, metabolomics approaches are limited

to excavating potential metabolites and associated pathways, without delving into direct relationships between these metabolites. Therefore, the novel strategy of combining metabolomics and network pharmacology, cross-talking upstream targets, pathways, and terminal metabolites, may provide a comprehensive and systematic view of the mechanisms involved in Cur therapy for AKI.

According to the molecular docking analysis, MAOA (identified from metabolomics and network pharmacology) exhibited the lowest binding energy with Cur (Table 2). MAOA is a mitochondrial metabolic enzyme that regulates the oxidative deamination of monoamine neurotransmitters and dietary amines, such as 5-HT. Previous studies have revealed a close association between AKI and MAOA-catalysed degradation of 5-HT.[44] Recently, it was reported that 5-HT exerts an anti-ferroptotic effect as a potent radical-trapping antioxidant.[10] Our results showed that MAOA in mice with AKI was inhibited by Cur, while the levels of 5-HT were increased in the Cur-treatment group (Figure 9). These findings imply that Cur also exerts an anti-ferroptotic effect in mice with AKI.

It was recently reported that regulated cell death (eg, necroptosis, apoptosis, and ferroptosis) contributes to different forms of tissue injury.[41] Ferroptosis is a type of programmed cell death distinguished by increased iron-dependent lipid peroxidation. Direct evidence has indicated that ferroptosis plays a critical role in the occurrence and development of AKI, as inhibitors of ferroptosis ameliorated renal injury in diverse animal models of AKI. Although Cur has received widespread attention in the treatment of different types of cancer by inducing anti-ferroptosis,[49,54,55] few studies thus far have explored the anti-ferroptotic effect of Cur. Treatment with Cur exhibited a significant anti-ferroptotic effect in HK2 cells, as well as reducing the elevated levels of MDA and iron in the kidneys of mice from the FA-treatment group (Figure 10). This evidence suggests that Cur exerts its anti-ferroptotic effect by regulating 5-HT metabolism via MAOA in AKI mice. Our findings in this study links ferroptosis to AKI development and identified important mediators that serves as effective targets in AKI.

Cur is suitable to be used in treating AKI induced by many factors in view of its safety, efficacy and very low toxic side effect profile, while whose limitations in clinical application exerts by the poor water solubility, low intestinal absorption efficiency, and low bioavailability in vivo.[50,56] For now, formulations techniques including nanoparticles, liposomes, and polymeric micelles contribute in improving bioavailability and enhancing the therapeutic effects of Cur, which improves the potential of Cur's clinical application.[57–59] Nevertheless, the combined use of curcumin and piperine indicating that co-administration of curcumin with other substances in clinical applications was also a useful method to improve its efficacy.[60] Thus, Cur nanoformulations or the co-administration maybe the further challenge to us in developing Cur as the candidates for clinical treatment of AKI.

Conclusion

In this research, we re-ensured the renoprotection of Cur in FA-induced AKI mice, and the ferroptosis-related injury in FA-AKI. Notably, we found that Cur ameliorated the ferroptosis-related injury in FA-AKI. Then, we screened MAOA as the key targets involved in the effects of Cur against FA-AKI using a combined metabolomics and network pharmacology approach. Furthermore, we confirmed that Cur regulates 5-HT metabolism through MAOA, thereby inhibiting ferroptosis in cells. These results suggest that the inhibition of ferroptosis is a potential mechanism by which Cur attenuates renal injury, and provides the basis for the development of new therapeutic strategies (such as Cur) for diseases related to ferroptosis, especially AKI.

Funding

This work was supported by Natural Science Foundation of Fujian Province, China (2023J05260); Major Science and Technology Projects by Natural Science Foundation of Fujian Province, China (No. 2022YZ035020); The Young Teachers Education Foundation of Fujian Province, China (No. JAT2200329); Innovation, Entrepreneurship, and Creation Education and Teaching Reform Research Project, Minjiang University (2022SCJG-03).

Disclosure

The authors reported no conflicts of interest in this work.

References

1. Turgut F, Awad AS, Abdel-Rahman EM. Acute kidney injury: medical causes and pathogenesis. *J Clin Med*. 2023;12(1):375. doi:10.3390/jcm12010375
2. Marx D, Metzger J, Pejchinovski M, et al. Proteomics and Metabolomics for AKI Diagnosis. *Semin Nephrol*. 2018;38(1):63–87. doi:10.1016/j.semnephrol.2017.09.007
3. Bellomo R, Kellum JA, Ronco C. Acute kidney injury. *Lancet*. 2012;380(9843):756–766. doi:10.1016/S0140-6736(11)61454-2
4. Chalkias A, Xanthos T. Acute kidney injury. *Lancet*. 2012;380(9857):1904. [author reply 1905]. doi:10.1016/S0140-6736(12)62104-7
5. Kumar S. Cellular and molecular pathways of renal repair after acute kidney injury. *Kidney Int*. 2018;93(1):27–40. doi:10.1016/j.kint.2017.07.030
6. Lin Q, Li S, Jiang N, et al. PINK1-parkin pathway of mitophagy protects against contrast-induced acute kidney injury via decreasing mitochondrial ROS and NLRP3 inflammasome activation. *Redox Biol*. 2019;26:101254. doi:10.1016/j.redox.2019.101254
7. Peerapornratana S, Manrique-Caballero CL, Gómez H, et al. Acute kidney injury from sepsis: current concepts, epidemiology, pathophysiology, prevention and treatment. *Kidney Int*. 2019;96(5):1083–1099. doi:10.1016/j.kint.2019.05.026
8. Chen HZ, Busse LW. Novel therapies for acute kidney injury. *Kidney Int Rep*. 2017;2(5):785–799. doi:10.1016/j.ekir.2017.06.020
9. Diego MS, Ruiz-Andres O, Poveda J, et al. Ferroptosis, but not necroptosis, is important in nephrotoxic folic acid–induced AKI. *J Am Soc Nephrol*. 2017;28(1):218–229. doi:10.1681/ASN.2015121376
10. Liu D, Liang C-H, Huang B, et al. Tryptophan metabolism acts as a new anti-ferroptotic pathway to mediate tumor growth. *Adv Sci (Weinh)*. 2023;10(6):e2204006. doi:10.1002/advs.202204006
11. Guo SS, Zhou L, Liu X, et al. Baicalein alleviates cisplatin-induced acute kidney injury by inhibiting ALOX12-dependent ferroptosis. *Phytomedicine*. 2024;130(2024):155757. doi:10.1016/j.phymed.2024.155757
12. Deng Y, Zeng L, Liu H, et al. Silibinin attenuates ferroptosis in acute kidney injury by targeting FTH1. *Redox Biol*. 2024;77:103360. doi:10.1016/j.redox.2024.103360
13. Li HD, Meng X-M, Huang C, et al. Application of herbal traditional Chinese medicine in the treatment of acute kidney injury. *Front Pharmacol*. 2019;10:376. doi:10.3389/fphar.2019.00376
14. Stepanić V, Kučerová-Chlupáčová M 2023 Review and chemoinformatic analysis of ferroptosis modulators with a focus on natural plant products. *Molecules* 282 475
15. Tsuda T. Curcumin as a functional food-derived factor: degradation products, metabolites, bioactivity, and future perspectives. *Food Funct*. 2018;9(2):705–714. doi:10.1039/C7FO01242J
16. Zhao YH, Shen C-F, Kang Y, et al. Curcumin prevents renal cell apoptosis in acute kidney injury in a rat model of dry-heat environment heatstroke via inhibition of the mitochondrial apoptotic pathway. *Exp Ther Med*. 2021;21(2):126. doi:10.3892/etm.2020.9558
17. Zhou J, Wu N, Lin L. Curcumin suppresses apoptosis and inflammation in hypoxia/reperfusion-exposed neurons via wnt signaling pathway. *Med Sci Monit*. 2020;26:e920445. doi:10.12659/MSM.920445
18. Gong X, Jiang L, Li W, et al. Curcumin induces apoptosis and autophagy inhuman renal cell carcinoma cells via Akt/mTOR suppression. *Bioengineered*. 2021;12(1):5017–5027. doi:10.1080/21655979.2021.1960765
19. Awad AS, El-Sharif AA. Curcumin immune-mediated and anti-apoptotic mechanisms protect against renal ischemia/reperfusion and distant organ induced injuries. *Int Immunopharmacol*. 2011;11(8):992–996. doi:10.1016/j.intimp.2011.02.015
20. Afrin MR, Arumugam S, Rahman MA, et al. Curcumin reduces the risk of chronic kidney damage in mice with nonalcoholic steatohepatitis by modulating endoplasmic reticulum stress and MAPK signaling. *Int Immunopharmacol*. 2017;49:161–167. doi:10.1016/j.intimp.2017.05.035
21. Ghelani H, Razmovski-Naumovski V, Chang D, et al. Chronic treatment of curcumin improves hepatic lipid metabolism and alleviates the renal damage in adenine-induced chronic kidney disease in Sprague-Dawley rats. *BMC Nephrol*. 2019;20(1):431. doi:10.1186/s12882-019-1621-6
22. Kar F, Hacioglu C, Senturk H, et al. Curcumin and LOXblock-1 ameliorate ischemia-reperfusion induced inflammation and acute kidney injury by suppressing the semaphorin-plexin pathway. *Life Sci*. 2020;256:118016. doi:10.1016/j.lfs.2020.118016
23. Wu TF, Marakkath B, Ye Y, et al. Curcumin attenuates both acute and chronic immune nephritis. *Int J Mol Sci*. 2020;21(5):1745.
24. Zhu H, Wang X, Wang X, et al. Curcumin attenuates inflammation and cell apoptosis through regulating NF-kappaB and JAK2/STAT3 signaling pathway against acute kidney injury. *Cell Cycle*. 2020;19(15):1941–1951. doi:10.1080/15384101.2020.1784599
25. Dastani M, Rahimi HR, Askari VR, et al. Three months of combination therapy with nano-curcumin reduces the inflammation and lipoprotein (a) in type 2 diabetic patients with mild to moderate coronary artery disease: evidence of a randomized, double-blinded, placebo-controlled clinical trial. *Biofactors*. 2023;49(1):108–118. doi:10.1002/biof.1874
26. Ramezani V, Ghadirian S, Shabani M, et al. Efficacy of curcumin for amelioration of radiotherapy-induced oral mucositis: a preliminary randomized controlled clinical trial. *BMC Cancer*. 2023;23(1):354. doi:10.1186/s12885-023-10730-8
27. Wei Z, Shaohuan Q, Pinfang K, et al. Curcumin attenuates ferroptosis-induced myocardial injury in diabetic cardiomyopathy through the Nrf2 pathway. *Cardiovasc Ther*. 2022;2022:3159717. doi:10.1155/2022/3159717
28. Jang C, Chen L, Rabinowitz JD. Metabolomics and Isotope Tracing. *Cell*. 2018;173(4):822–837. doi:10.1016/j.cell.2018.03.055
29. Johnson CH, Ivanisevic J, Siuzdak G. Metabolomics: beyond biomarkers and towards mechanisms. *Nat Rev Mol Cell Biol*. 2016;17(7):451–459. doi:10.1038/nrm.2016.25
30. Nicholson JK, Lindon JC, Holmes E. 'Metabonomics': understanding the metabolic responses of living systems to pathophysiological stimuli via multivariate statistical analysis of biological NMR spectroscopic data. *Xenobiotica*. 1999;29(11):1181–1189. doi:10.1080/004982599238047
31. Konjevod M, Nedic Erjavec G, Nikolac Perkovic M, et al. Metabolomics in posttraumatic stress disorder: untargeted metabolomic analysis of plasma samples from Croatian war veterans. *Free Radic Biol Med*. 2021;162:636–641. doi:10.1016/j.freeradbiomed.2020.11.024
32. Konjevod M, Tudor L, Svob Strac D, et al. Metabolomic and glycomic findings in posttraumatic stress disorder. *Prog Neuro Psychopharmacol Biol Psychiatry*. 2019;88:181–193. doi:10.1016/j.pnpbp.2018.07.014
33. Zhou Y, Lu R, Lin F, et al. Exploring the therapeutic potential of ethyl 3-hydroxybutyrate in alleviating skeletal muscle wasting in cancer cachexia. *Biomolecules*. 2023;13(9):1330. doi:10.3390/biom13091330
34. Chen Y, Lu T, Pettersson-Kymmer U, et al. Genomic atlas of the plasma metabolome prioritizes metabolites implicated in human diseases. *Nat Genet*. 2023;55(1):44–53. doi:10.1038/s41588-022-01270-1

35. Li Q, Xing C, Yuan Y. Mitochondrial targeting of herbal medicine in chronic kidney disease. *Front Pharmacol*. 2021;12:632388. doi:10.3389/fphar.2021.632388
36. Hopkins AL. Network pharmacology. *Nat Biotechnol*. 2007;25(10):1110–1111. doi:10.1038/nbt1007-1110
37. Hopkins AL. Network pharmacology: the next paradigm in drug discovery. *Nat Chem Biol*. 2008;4(11):682–690. doi:10.1038/nchembio.118
38. Tao C, Wang J, Gu Z, et al. Network pharmacology and metabolomics elucidate the underlying mechanisms of Venenum Bufonis in the treatment of colorectal cancer. *J Ethnopharmacol*. 2023;317:116695. doi:10.1016/j.jep.2023.116695
39. Mao T, Xie L, Guo Y, et al. Mechanistic exploration of Yiqi Liangxue Shengji prescription on restenosis after balloon injury by integrating metabolomics with network pharmacology. *Pharm Biol*. 2023;61(1):1260–1273. doi:10.1080/13880209.2023.2244533
40. Li T, Zhang W, Hu E, et al. Integrated metabolomics and network pharmacology to reveal the mechanisms of hydroxysafflor yellow A against acute traumatic brain injury. *Comput Struct Biotechnol J*. 2021;19:1002–1013. doi:10.1016/j.csbj.2021.01.033
41. Wang Y, Quan F, Cao Q, et al. Quercetin alleviates acute kidney injury by inhibiting ferroptosis. *J Adv Res*. 2020;28:231–243. doi:10.1016/j.jare.2020.07.007
42. Metz-Kurschel U, Kurschel E, Wagner K, et al. Folate nephropathy occurring during cytotoxic chemotherapy with high-dose folinic acid and 5-fluorouracil. *Ren Fail*. 1990;12(2):93–97. doi:10.3109/08860229009087124
43. Yan LJ. Folic acid-induced animal model of kidney disease. *Animal Model Exp Med*. 2021;4(4):329–342. doi:10.1002/ame2.12194
44. Jin JQ, Xu F, Zhang Y, et al. Renal ischemia/reperfusion injury in rats is probably due to the activation of the 5-HT degradation system in proximal renal tubular epithelial cells. *Life Sci*. 2021;285:120002.
45. Hu Z, Zhang H, Yi B, et al. VDR activation attenuate cisplatin induced AKI by inhibiting ferroptosis. *Cell Death Dis*. 2020;11(1):73. doi:10.1038/s41419-020-2256-z
46. Cai FF, Li D, Zhou K, et al. Tiliroside attenuates acute kidney injury by inhibiting ferroptosis through the disruption of NRF2-KEAP1 interaction. *Phytomedicine*. 2024;126:155407. doi:10.1016/j.phymed.2024.155407
47. Li W, Xiang Z, Xing Y, et al. Mitochondria bridge HIF signaling and ferroptosis blockage in acute kidney injury. *Cell Death Dis*. 2022;13(4):308. doi:10.1038/s41419-022-04770-4
48. Tang X, Ding H, Liang M, et al. Curcumin induces ferroptosis in non-small-cell lung cancer via activating autophagy. *Thorac Cancer*. 2021;12(8):1219–1230. doi:10.1111/1759-7714.13904
49. Wu L, Dong B, Chen Q et al. Effects of curcumin on oxidative stress and ferroptosis in acute ammonia stress-induced liver injury in gibel carp (Carassius gibelio). *Int J Mol Sci*. 2023;24(7):6441.
50. Abbasi S, Sato Y, Kajimoto K, et al. New design strategies for controlling the rate of hydrophobic drug release from nanoemulsions in blood circulation. *Mol Pharm*. 2020;17(10):3773–3782. doi:10.1021/acs.molpharmaceut.0c00542
51. Wu J, Pan X, Fu H, et al. Effect of curcumin on glycerol-induced acute kidney injury in rats. *Sci Rep*. 2017;7(1):10114. doi:10.1038/s41598-017-10693-4
52. El-Gizawy MM, Hosny EN, Mourad HH, et al. Curcumin nanoparticles ameliorate hepatotoxicity and nephrotoxicity induced by cisplatin in rats. *Naunyn Schmiedebergs Arch Pharmacol*. 2020;393(10):1941–1953. doi:10.1007/s00210-020-01888-0
53. Kumar P, Sulakhiya K, Barua CC, et al. TNF-alpha, IL-6 and IL-10 expressions, responsible for disparity in action of curcumin against cisplatin-induced nephrotoxicity in rats. *Mol Cell Biochem*. 2017;431(1–2):113–122. doi:10.1007/s11010-017-2981-5
54. Cao X, Li Y, Wang Y, et al. Curcumin suppresses tumorigenesis by ferroptosis in breast cancer. *PLoS One*. 2022;17(1):e0261370. doi:10.1371/journal.pone.0261370
55. Chen M, Tan AH, Li J. Curcumin represses colorectal cancer cell proliferation by triggering ferroptosis via PI3K/Akt/mTOR Signaling. *Nutr Cancer*. 2023;75(2):726–733. doi:10.1080/01635581.2022.2139398
56. Cai Y, Huang C, Zhou M, et al. Role of curcumin in the treatment of acute kidney injury: research challenges and opportunities. *Phytomedicine*. 2022;104:154306. doi:10.1016/j.phymed.2022.154306
57. Feng T, Wei Y, Lee R, et al. Liposomal curcumin and its application in cancer. *Int J Nanomed*. 2017;12:6027–6044. doi:10.2147/IJN.S132434
58. Huang M, Liang C, Tan C, et al. Liposome co-encapsulation as a strategy for the delivery of curcumin and resveratrol. *Food Funct*. 2019;10(10):6447–6458. doi:10.1039/C9FO01338E
59. Jardim KV, Siqueira JLN, Báo SN, et al. The role of the lecithin addition in the properties and cytotoxic activity of chitosan and chondroitin sulfate nanoparticles containing curcumin. *Carbohydr Polym*. 2020;227:115351. doi:10.1016/j.carbpol.2019.115351
60. Shoba G, Joy D, Joseph T, et al. Influence of piperine on the pharmacokinetics of curcumin in animals and human volunteers. *Planta med*. 1998;64(4):353–356. doi:10.1055/s-2006-957450